sustainability

MDPI

Article

Investigation of Load-Bearing Capacity for Reinforced Concrete Foundation Retrofitted Using Steel Strut–Tie Retrofit System

Jiuk Shin [1] and Kihak Lee [2,*]

[1] Department of Architectural Engineering, Gyeongsang National University (GNU), 501 Jinju-daero, Jinju-si 52828, Republic of Korea; jiukshin@gnu.ac.kr
[2] Department of Architectural Engineering, Sejong University, 209 Neungdong-ro, Gwangjin-gu, Seoul 05006, Republic of Korea
* Correspondence: kihaklee@sejong.ac.kr

Abstract: To reduce the thickness of reinforced concrete foundation members used in construction and structural applications, a previous study developed and tested a strut–tie retrofit system installed in the foundations. This study proposes the optimum retrofit details of a steel-tie retrofit system for foundation members with reduced thickness via a finite element simulation-based load-bearing capacity assessment. The retrofit parameters (structural steel type, plate thickness, and number of strut frames) that significantly affected the load-bearing capacities were optimized by comparing the maximum effective stress and code-defined allowable stress limits. The optimum retrofit details were compared with those computed using a code-defined strut–tie model. Based on the load-bearing capacity assessment for the design of loading combinations, the optimum retrofit details can be reduced in transverse (by 55%) and longitudinal (by 87%) directions compared with those designed using the strut–tie model approach.

Keywords: reinforced concrete foundation; steel strut–tie retrofit system; load-bearing capacity assessment; nonlinear finite element simulation

check for updates

Citation: Shin, J.; Lee, K. Investigation of Load-Bearing Capacity for Reinforced Concrete Foundation Retrofitted Using Steel Strut–Tie Retrofit System. *Sustainability* **2023**, *15*, 10372. https://doi.org/10.3390/su151310372

Academic Editors: Igor Martek and Mehdi Amirkhani

Received: 5 April 2023
Revised: 16 June 2023
Accepted: 27 June 2023
Published: 30 June 2023

1. Introduction

1.1. Background

In general, the foundation members of bridges and building structures that are in direct contact with soil transmit shear and bending moments from the structures to the soil. Because building and bridge structures have recently become larger, the loads acting on foundation members have increased significantly. The increased loads, in turn, increased the thickness of the foundation members. In particular, the foundation members that resisted various loading types (e.g., axial force, shear force, and bending moment) acting on the column bases suffered from stress concentration, which contributed to an increase in the thickness of the foundation [1,2].

An increase in thickness of the foundation can lead to the following problems: (1) extensive ground excavation; (2) an increase in steel reinforcing bars; (3) thermal cracks in concrete; and (4) extensive CO_2 emissions [1–8]. Owing to the increase in thickness of the foundation, the volume of excavation must be increased, which leads to technical difficulties (e.g., rock crushing, equipment movement, and backfilling) during construction [3]. For deep foundation members, the number of steel reinforcing bars that resist the loads acting on the column bases needs to be significantly increased compared with other foundations. Accordingly, the labor and construction periods can be increased to manufacture a large number of reinforcing bars. Another problem is the control of thermal cracks in concrete members. During the concrete's curing time, the hydration heated in the foundation members is emitted; consequently, the hydration heat emissions produce the thermal cracks in the concrete. To control thermal cracks occurring in deep foundation members, a pipe cooling system that decreases hydration heat is often installed [4]. This additional process can lead to longer construction periods and higher costs. Finally, the extensive use of concrete materials owing to the increase in foundation depth causes an environmental impact because the production of the concrete material (raw material cement) is energy-intensive and generates a large amount of emissions of CO_2 [5,6]. Therefore, a method to reduce the thickness of the foundation is required.

In previous research [1], a steel strut-type retrofit system installed in the foundation was developed to resolve the structural and construction problems in foundations. Using this retrofit system, the localized concentrated load acting on the pier was uniformly distributed to the ground throughout the foundation. This retrofit method entailed the formation of a steel plate with higher strength and machinability than concrete into an arch and its installation on the base of the columns. Tension ties fixing the arch shape were prefabricated into a unit with the strut-type retrofit system and installed at the base of the columns to reduce the thickness of the foundation. Subsequently, the excavation and construction time for the foundation could be reduced because of the decreased amount of concrete and reinforcing steel. The use of jet-grouted micropiles in foundation members enhances the mechanical properties of soils and mitigates the liquefaction potentials induced by seismic loads. The effectiveness of this novel approach was verified using cone penetration test (CPT) and a standard penetration test (SPT)-based liquefaction assessment methods [9]. A previous study [6] investigated the load-bearing capacities of piled raft foundations (PRFs) with respect to various parameters (pile length, pile diameter, and raft thickness) using finite element (FE) analyses. A previous numerical study [10] demonstrated that the selected parameters significantly affected the reduction in the total and differential settlements, as well as the shear and bending moments on the raft. Recently, Stone et al. [11] optimized the details of a new composite foundation system with a caliche-stiffened pile (CSP) based on FE simulations. The optimum pile length was proposed without enhancing soil properties in a cost-effective manner. In addition, the CSP foundation member can reduce pile settlement.

The strut retrofit system used in this study represents the shape of the strut–tie model (STM) formed by the loads acting on the member. Figure 1 shows the basic configuration of the strut retrofit system. The arch-shaped strut frame transfers the compressive force acting on the column to the base of the foundation. The tie bar is installed to resist bending and tension [12,13]. In this study, we investigated the foundation member where the steel strut–tie retrofit system was applied. The results showed that the steel strut reinforcement improved the strength by over 60% compared with non-retrofitted foundation members. Thus, it was demonstrated that the strut reinforcement was effective in reducing the thickness of the foundation.

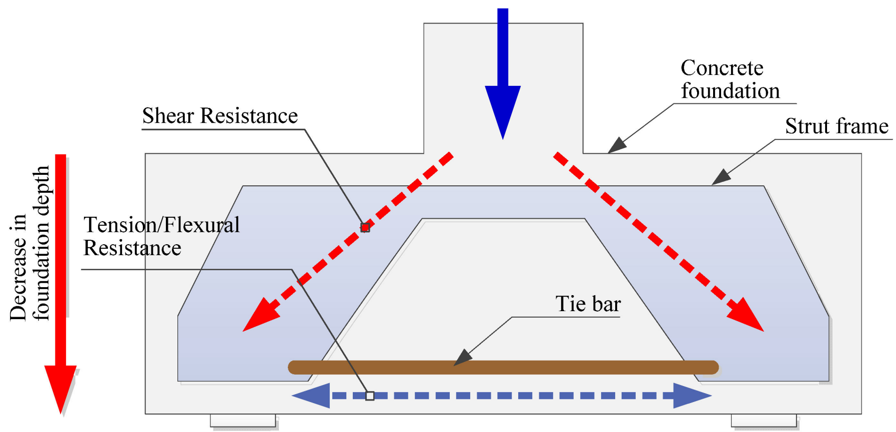

Figure 1. Reinforced concrete foundation installed with a strut–tie retrofit system.

The steel strut retrofit system used in this study was designed using the STM method for the load acting on the steel concrete column. The STM method is a truss model that is based on the application of plasticity theory and force equilibrium conditions. It is an efficient method for shear design in the load disturbance zone of a member [14]. The STM method accurately identifies the force flow. Therefore, the load-bearing capacity of the load disturbance zones can be determined more reasonably.

1.2. Research Purpose

This study proposes the optimum details of a steel strut–tie retrofit system for foundation members through a load-bearing capacity assessment. To accomplish this, a strut retrofit system with a thickness equal to 80% of that of a typical RC foundation was designed for mat and pile foundations using the STM method. Subsequently, a nonlinear FE analysis was conducted for an RC foundation incorporating a strut retrofit system. Furthermore, the load-bearing capacities of the foundation members were evaluated regarding the flexural moment and shear force. In addition, optimum retrofit parameters for the strut plate thickness that significantly affect the flexural performance were recommended for the given loading scenarios.

2. Design of Steel Strut Using Strut and Tie Model

2.1. Strut and Tie Model Approach

The STM approach is a shear design method that applies the truss model. It is formed based on the force flow and load distribution that are generated when a load is applied to a structure. As shown in Figure 2, the STM is composed of the strut, representing the compressive force of the structure, the tie, representing the tensile forces, and the nodal region where the strut and tie come in contact. This design method is applied in RC structural members with complex load distributions owing to corbels, joints, and deep beams. This method designs the structural details based on the load distribution. Therefore, it facilitates the application of new designs unlike conventional empirical equations derived from experimental studies [15–17]. In this study, a strut–tie retrofit system was designed according to the loading distribution on the foundation elements (unlike conventional foundation members composed of concrete, flexural, and shear reinforcements) and applied on the foundation within the concrete. Therefore, the thickness of the foundation could be reduced, compared with the case in which the conventional design method specified in current design codes was used [14,18], while maintaining the shear resistance performance.

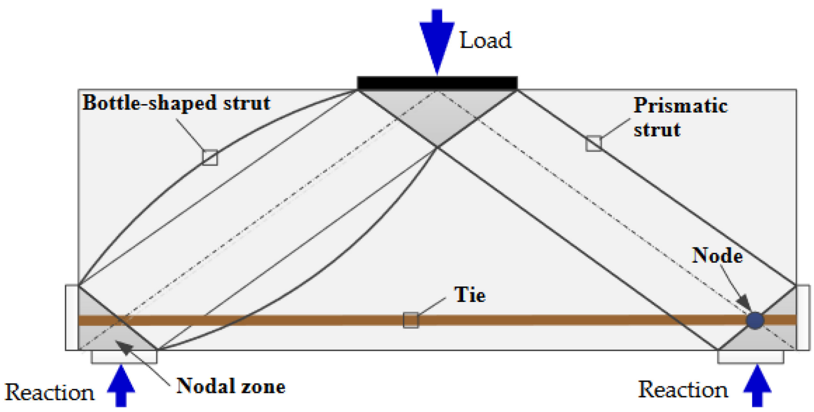

Figure 2. Strut–tie model (STM) in reinforced concrete member.

This study applies the existing STM design method to design a strut–tie retrofit system that can resist flexure and shear forces acting on the foundation. The application procedure of the design method is as follows:

(1) Develop an FE model to analyze the stress distribution for the given load combinations without the strut retrofit system.
(2) Propose a truss model (STM) for the longitudinal and transverse directions in a bridge structure based on the stress distribution of the FE model (STM shape determination).

(3) Calculate the axial forces of the compression and tension members of the truss model for each load combination.
(4) Design the strut based on the compressive axial forces (determine the required cross-sectional width and calculate the required number of struts).
(5) Design the tie based on the tensile force of the tension member (design the steel wire and reinforcement).

2.2. Design Process of Steel Struts and Ties

This section describes the design of a strut–tie stiffener for the load combinations presented in Table 1 according to the five-step design process mentioned in Section 2.1. The design information of the foundation considered in this study is presented in Table 2.

Table 1. Information on loading combinations in transverse and longitudinal directions.

Classification		Loading Combination	Shear (kN)	Axial Load (kN)	Moment (kN-m)
Transvers direction	Maximum axial load	LC-1	1265	54,229	21,027
	Maximum moment	LC-2	1265	51,656	21,027
	Earthquake	LC-3	2968	54,519	52,527
Longitudinal direction	Maximum axial load	LC-1	2431	54,229	180
	Maximum moment	LC-2	119	50,508	1945
	Earthquake	LC-3	5133	54,519	51,140

Table 2. Summary of design information of foundation.

Concrete Strength (f_{ck}, MPa)	Steel Reinforcing Bar		Steel Type	Tie (Steel Wire)		Foundation Thickness (mm)
	Yielding Strength (f_{sy}, MPa)	Diameter (mm)		Tensile Strength (f_{pu}, MPa)	Diameter (mm)	
35	400	29	SM490	1100	32	2000 (80% of typical foundation thickness)

Figure 3 presents an elastic FE model consisting of solid elements developed to estimate the loading distribution of the concrete foundation model subjected to the load combinations. LS-DYNA [19], a commercial nonlinear FE analysis program, was used to develop the FE model. The elastic FE model was modeled with the following dimensions: 7400 × 16,900 mm (the transverse and longitudinal directions, respectively). The thickness of the foundation was set to 2000 mm. This was 80% of that (2500 mm) computed using the conventional design method. Figure 3 presents an example of the loading distribution on the pile and mat foundations for the LC1-load combination. For the stress distribution, the sections on which the maximum effective stresses acted were analyzed. As shown in the figure, the stress was distributed diagonally along the depth of the foundation member relative to the loading point. It can be clarified that unlike the mat foundation, the stress within the concrete element (solid component) is distributed along the pile because the stress of the pile foundation is transferred to the piles.

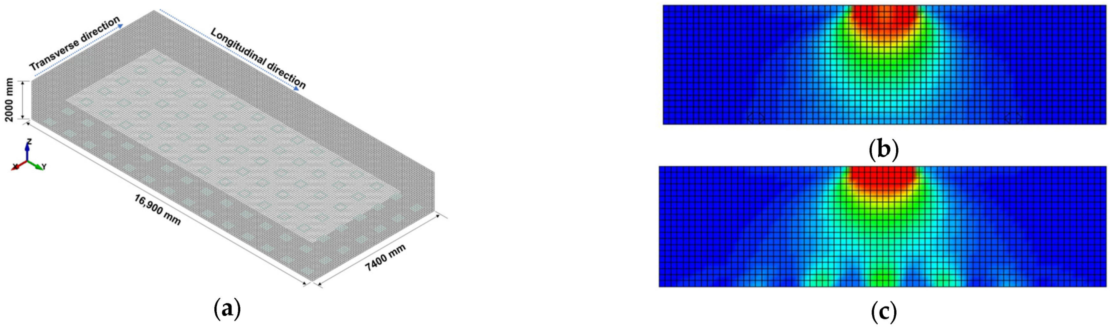

Figure 3. FE model with elastic material and effective stress distribution in the transverse direction. (**a**) Geometric finite element model. (**b**) Mat-type foundation. (**c**) Pile-type foundation.

The diagonal strut width (w_{sb}) was determined in order to design the strut frame. Here, θ indicates the angle between the strut and tension member of the foundation member. The width of the strut was determined as shown in Equation (1). Here, w_t is the tie width and l_b is the width of the tension point or support plate.

$$w_{sb} = w_t cos\theta + l_b sin\theta \tag{1}$$

In this design, the required member width (w_{req}) can be determined using the relationship between the member force and load (see Equation (2)). Here, β_s is the coefficient that considers the effect of the tie anchoring at the nodal point for the effective compressive strength of concrete. The bearing capacity of an individual strut can be calculated using Equation (3). The external force (axial force of truss member, F_u) and internal force (ϕF_{ns}) are compared to determine the number of strut members. The A_s (the total area of steel reinforcing bars) in Equation (3) represents the distance between the points (bs) upon multiplication with the thickness of the strut stiffener plate (t_{pl}).

$$w_{req} = F_u \ / \ (\phi 0.85 \ \beta_s \ f_{ck} \ bs) \tag{2}$$

$$\phi F_{nz} = (\phi 0.85 \ \beta_s \ f_{ck} \ w_{sb} bs + A_s f_y) \tag{3}$$

Finally, to design the strut member, the number of strut members is computed by comparing the required width (w_{req}) with the actual width (w_{sb}) of the strut. Based on this design, the required number of strut–tie frames for the LC-1 load combination in the transverse direction was calculated as four when the plate thickness was assumed to be 40 mm. Similarly, the number of required frames for the strut–tie retrofit design in the longitudinal direction was calculated to be three when the plate thickness was assumed to be 40 mm.

Finally, the tension ties were designed based on the axial force of the tension member calculated using the structural analysis of the truss model. The tension member comprises the steel wire and reinforcing bar connected to the strut–tie retrofit system. Equation (4) can be used to determine the number of steel wires (A_t) and reinforcement (A_s) based on the tensile force.

$$\phi f_{nt} = \left(A_s \ f_{sy} + A_t \ f_{ty}\right) \tag{4}$$

Table 3 summarizes the results for the strut–tie retrofit system determined using the strut–tie design method. The number of strut frames was calculated by modifying the plate thickness (t_{pl}).

Table 3. Summary of design information for strut–tie retrofitted foundation.

Direction	f_{ck} (MPa)	Size (mm)	Thickness (mm)	Strut Frame				Tie		
				Steel Type	Yielding Strength (MPa)	Plate Thickness (t_{pl}, mm)	Required Number	Tensile Strength (MPa)	Wire Diameter (mm)	Required Number
Transverse direction	35	7400	2000	SM490	315	40	8	1100	32	16
Longitudinal direction		16,900					3	1100	32	6

3. Finite Element Model

Figure 4 illustrates the geometric, material, and elemental information on the pile-type FE foundation model installed with the strut–tie retrofit system. The pile-type FE foundation model was fixed on the rigid elements in the all-direction sample representing the foundation piles. The mat-type FE foundation model differs from the pile-type model only in terms of the boundary condition location. The boundary condition on the mat-type model was adapted so the entire base resisted the load, excluding the rigid elements installed at the foundation base from the pile-type model. The solid elements composed of eight nodes were used for the concrete. The mesh size was set to 100 mm considering the computational time. The steel reinforcement was modeled with the Hughes–Liu beam element composed of two nodes, and the nodes of the reinforcement were separated from the concrete mesh nodes.

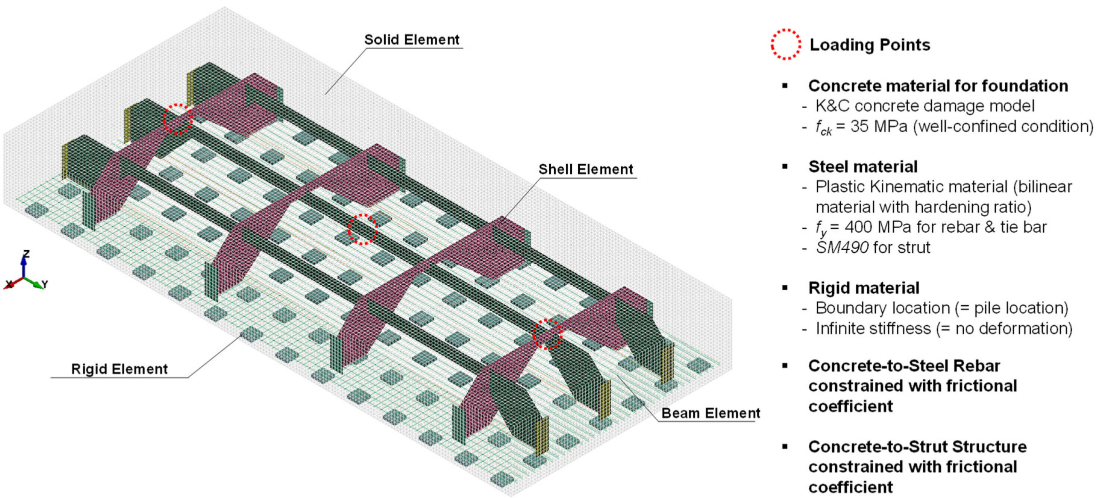

Figure 4. Pile-type finite element foundation model.

The concrete damage model of LS-DYNA (Karagozian and Case concrete model, KCC model) [20,21] was applied for the concrete material model used in this study. The KCC model has been widely used to analyze the element or building levels for explosions and earthquake loads. It can implement complex effects of confinement, strain hardening/softening, shear dilation, and stiffness reduction. The steel reinforcement was set to SD400 (f_{sy} = 400 MPa), and the steel type of the strut frame was initially set to SM490 (f_{ry} = 315 MPa). The yielding strength of the tie reinforcement was assumed to be 400 MPa. The plastic kinematic material model was used to depict the bilinear behavior of the reinforcement and strut frame, and the ultimate strength was reflected for the strain hardening. Tables 4 and 5 summarize the main material properties of concrete and steel reinforcing bars.

Table 4. Main parameters of concrete material.

Poisson's Ratio	Density (g/mm^3)	Compressive Strength (MPa)	Tensile Strength (MPa)	Elastic Modulus (MPa)	Max. Aggregate Size (mm)	Dilation Factor
0.16	0.0023	35	2.69	29937.9	6.35	0.8

Table 5. Main parameters of steel reinforcement material.

Type	Poisson's Ratio	Density (g/mm^3)	Elastic Modulus (MPa)	Yield Strength (MPa)	Ultimate Strength (MPa)
D29 rebar	0.3	0.0078	206,000	400	512
SM490 strut	0.3	0.0078	206,000	315	490
φ47 steel wire	0.3	0.0078	206,000	400	512

The bonding condition between the beam elements and the surrounding concrete solid elements was modeled using the Constrained_Lagrange_In_Solid function of LS-DYNA. It can connect two models with the frictional force. This was conducted to develop the bond-slip effects that may occur after concrete damage occurs between the reinforcing bars and surrounding concrete. In general, the modeling approach shares nodes between the steel reinforcement and concrete models (node combination between two models). It effectively bonded the two models to depict the integrated behavior between the reinforcement and concrete models regardless of the concrete damage. Moreover, the method may exaggerate the behavior of RC structures. The FE models developed in this study implement the Constrained_Lagrange_In_Solid function that can reproduce the behavior between concrete and reinforcement with a friction coefficient to generate a realistic behavior between these elements [22–24]. The strut model from the strut–tie retrofit system was developed using a shell-type element with a mesh size of 100 mm. The beam element was utilized for the tie models (steel wire). The shell elements for the strut model set as a slave were coupled with the concrete solid elements set as a master using the Constrained_Shell_In_Solid function, which can control the bonding strength with the frictional coefficient. The steel reinforcing bars and steel strut–tie retrofit details in the FE foundation models were constrained using frictional forces between those steel materials and the surrounding concrete materials.

In this study, the boundary condition was differentiated to model the pile and mat foundations. A rigid element with infinite stiffness was used to model the location of the pile in the pile foundation. The boundary condition of each rigid component was set to be constrained in all the directions. In the mat foundation, the boundary conditions were set such that the bottom surface of the solid elements of the foundation could be constrained from all directions without rigid elements. To evaluate the serviceability of the strut–tie retrofit system, the service loads were applied to each load combination presented in Table 1, and a static nonlinear analysis was performed subjected to the loads. The loading locations in the FE model are indicated using a dotted red line in Figure 4. The loading locations were determined based on the pier shape.

4. Load-Bearing Capacity Assessment

4.1. Flexure Assessment

The FE models developed for the pile and mat foundations were used to perform a static nonlinear analysis for the service (design) loads presented in Table 1. The initial FE foundation models were designed according to the strut–tie design method. Here, the strut plate thickness (t_{pl}) was 40 mm, and the material was assumed to be SM490. In this section, the von Mises (VM) stress (effective stress) was evaluated based on the results of the FE analysis for the service loads. Consequently, the maximum effective stress computed from the VM stress distributions was used to determine the steel material type and plate thickness of the strut depending on whether the maximum effective stress of the steel strut exceeded the allowable stress limits specified in the design guidelines [25].

Figure 5 shows the VM stress distribution of the strut frame for the initial FE foundation models (with t_{pl} = 40 mm) computed with the nonlinear static analyses for each load combination. As presented in the figures, the maximum effective stress was observed in the transverse direction of the strut frame regardless of the load combination, and the stress concentration was detected at the loading points.

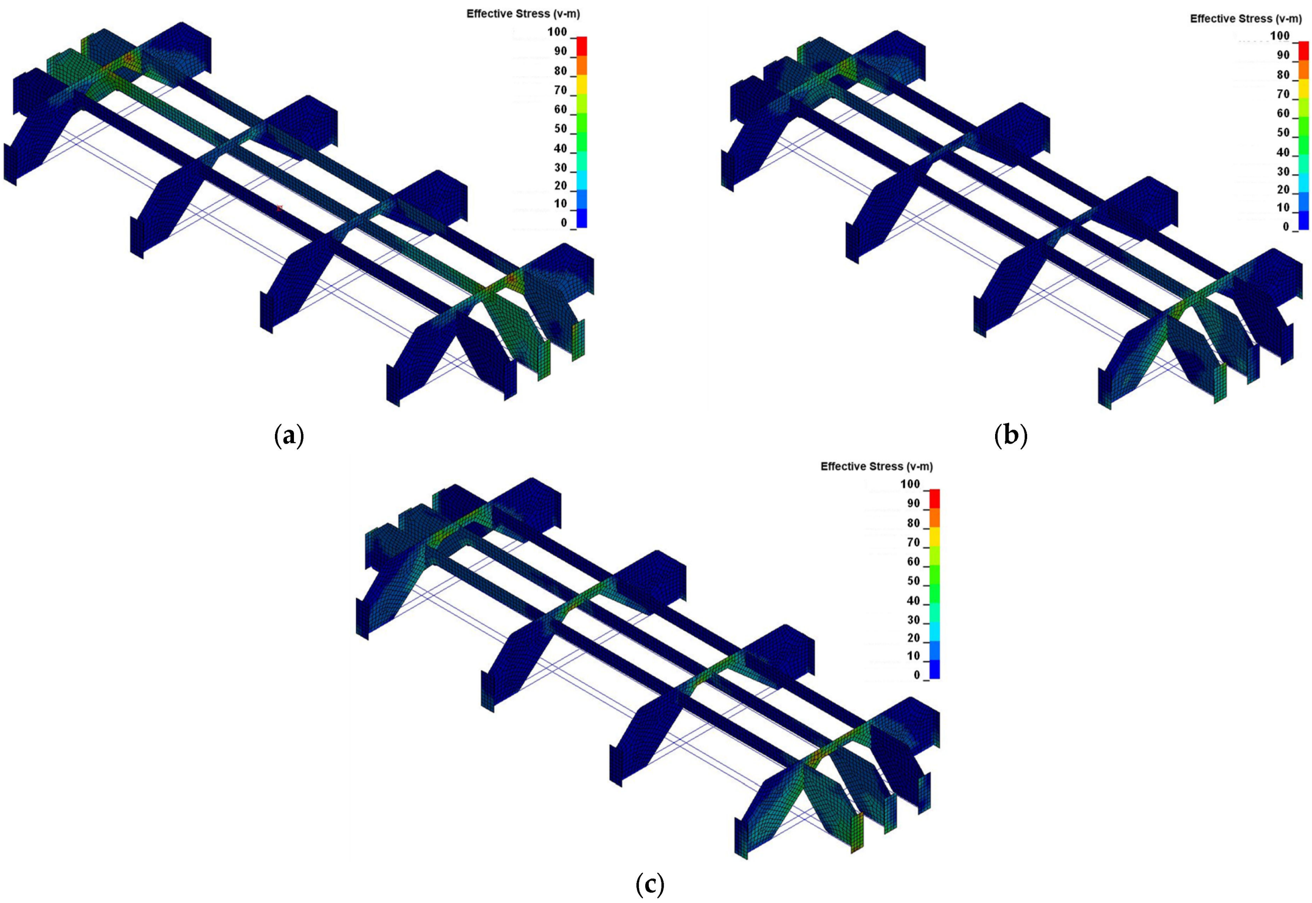

Figure 5. Effective stress distribution of strut–tie retrofit system. (**a**) LC-1. (**b**) LC-2. (**c**) LC-3.

The nonlinear static analyses of the FE foundation models while reducing t_{pl} from 40 mm to 10 mm were performed for each loading combination. Based on the FE simulations, the maximum effective stress for each loading scenario was compared with the permissible stress of structural steel (see Table 6), which was in compliance with the Railway Design Standard of the Ministry of Land, Infrastructure, and Transport published in 2015 [25].

Table 6. Summary of allowable stress for structural steel type [25].

Stress Type	Plate Thickness	SS400 SM400 SMA400	SM490	SM490Y SM520 SMA490	SM580 SMA570
Axial stress	≤40 mm	140 MPa	190 MPa	215 MPa	270 MPa
Flexural stress	≤40 mm	140 MPa	190 MPa	215 MPa	270 MPa

Figure 6 shows the relationship between the maximum effective stress and strut plate thickness for the pile and mat foundations in the LC-1 loading combination. Only the LC-1 loading scenario is presented in this paper because the maximum effective stress of the strut–tie retrofit system is observed in LC-1 among the loading combinations considered in this study. To determine the type of structural steel for the strut frame, the permissible stresses of SM490 and SS400 structural steels are also included in the figure. Overall, the maximum effective stress shown in the pile foundation model was higher than that for the mat foundation for all the loading combinations considered. Therefore, in this study, the plate thickness of the strut frame and type of structural steel were selected based on the LC-1 load combination for the pile foundation model by comparing the FE simulation-based VM stress with the code-defined permissible stresses. In addition, the reduction in the plate thickness caused the VM stress values on the strut–tie retrofit system to increase. This indicates that the initially assumed plate thickness (t_{pl} = 40 mm) can be reduced until the VM stress values are close to the permissible stress value to optimize the strut frame details.

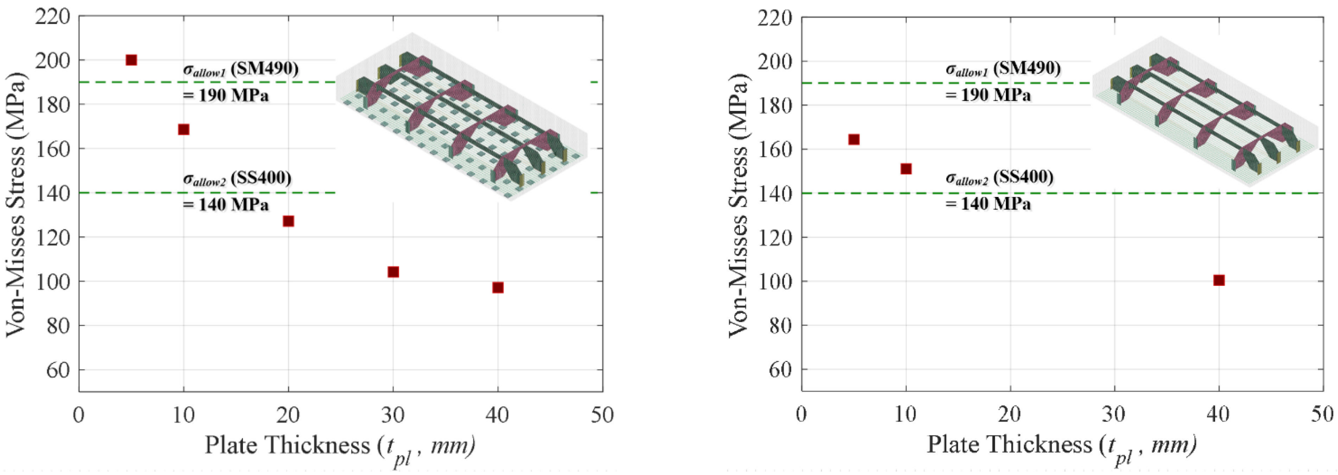

(**a**) (**b**)

Figure 6. Maximum effective stress of strut frame with respect to plate thickness. (**a**) Pile-type. (**b**) Mat-type.

Figure 7 shows the maximum effective stress results with varying plate thickness for all the load combinations. For SS400 steel, the minimum plate thickness for the effective stress on the strut frame to be within the allowable stress was required to be at least 17 mm for the service loading scenarios. The optimum plate thickness computed using the FE simulations (FE simulation-based design method) was approximately 45% of the strut plate thickness (t_{pl} = 40 mm), which was determined based on the strut–tie design method. The FE simulation-based design method that determines the strut frame details considering the actual structural behavior is highly effective in reducing the material quantity as compared to the conventional code-defined design method.

The FE simulation-based design method introduced in this section significantly reduced the material quantity in the strut frame compared with the conventional code-defined design method. In addition, the maximum effective stress of the strut frame in the longitudinal direction was smaller than that in the transverse direction. Section 4.2 describes the implementation of the FE simulation-based design method considering the effective stress distribution, which can reduce the number of strut frames in the longitudinal direction, and further proposes the optimal strut–tie retrofit system.

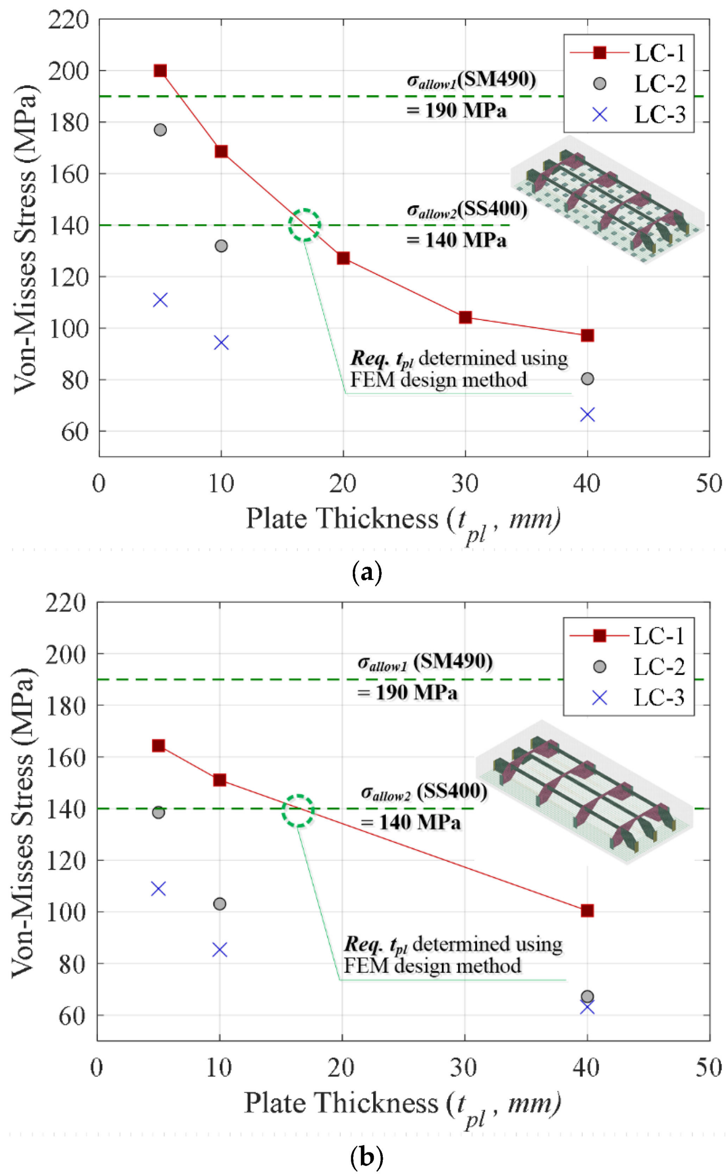

Figure 7. Required plate thickness with respect to maximum effective stress. (**a**) Pile-type. (**b**) Mat-type.

4.2. FE-Simulation-Based Optimum Details

Figure 8 summarizes the procedure for deriving the optimum retrofit details. The initial retrofit details were proposed using the STM-based approach. Moreover, the retrofit details regarding the number of the strut frames and plate thickness were optimized using the flexural assessment. The flexural stress values computed using the FE foundation models with various strut frame numbers and plate thickness were compared to the code-defined allowable limits. After that, the FE foundation models with the optimum retrofit details were used to calculate the shear force with respect to the design loading combinations. The mean value of shear stress simulated from the FE models was compared with the allowable limits in transverse and longitudinal directions.

This section describes the estimation of the VM stress distribution (described in Section 4.1) of the FE foundation models after the number of strut–tie retrofit systems in the longitudinal direction is reduced from three to two. The LC-1 loading combination where the maximum stress values were found among the all-loading combinations was applied to the FE foundation models. The maximum effective stress of the FE models with the reduced plate thickness was compared with the code-defined allowable stress limits for each type of structural steel.

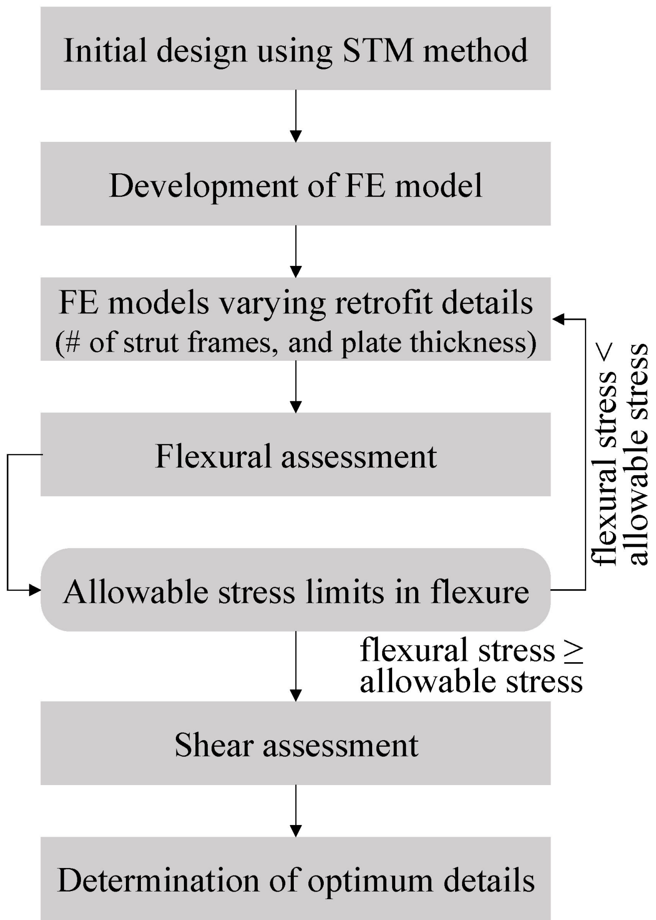

Figure 8. Optimum design procedure of strut–tie retrofit system.

Figure 9 shows the maximum effective stress of the FE foundation models under the LC-1 loading combination when the plate thickness was decreased from 40 mm to 10 mm. After the number of strut–tie retrofit systems (from three to two) was reduced, the plate thickness of the strut frame was set to approximately 18 mm so that the stress was close to the permissible stress of SS400. Using this FE-based design method, the required number of strut–tie retrofit systems in the transverse and longitudinal directions was determined to be four and two, respectively, and the required plate thickness of the strut frame was determined to be 18 mm. The detailed information regarding the reduced retrofit system is provided in Table 7.

Following the determination of the retrofit details of the strut–tie system, because the effective stress of the strut frame in the longitudinal direction was significantly lower than that of the strut frame in the transverse direction, the retrofit system was optimized by reducing the plate thickness of the strut frame in the longitudinal direction.

Figure 9 shows the effective stress of the FE foundation models after the plate thickness of the strut frame in the longitudinal direction is reduced to 8 mm. The plate thickness of the strut frame in the longitudinal direction was determined based on FE simulations with varying thickness values of the strut frame. Figure 9a illustrates the pile-type FE foundation model with the optimum plate thickness of the strut frame. As shown in Figure 9b, the maximum effective stress values of the strut frame in the longitudinal and transverse directions were less than the permissible stress (140 MPa) of SS400 structural steel notwithstanding the reduced plate thickness in the longitudinal direction.

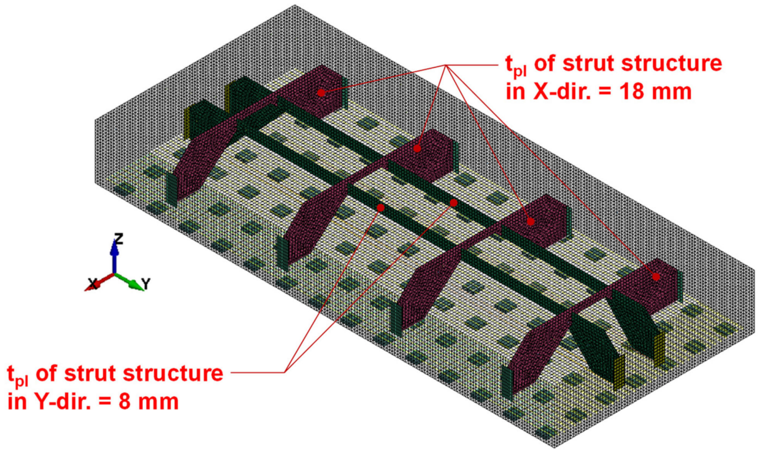

(**a**)

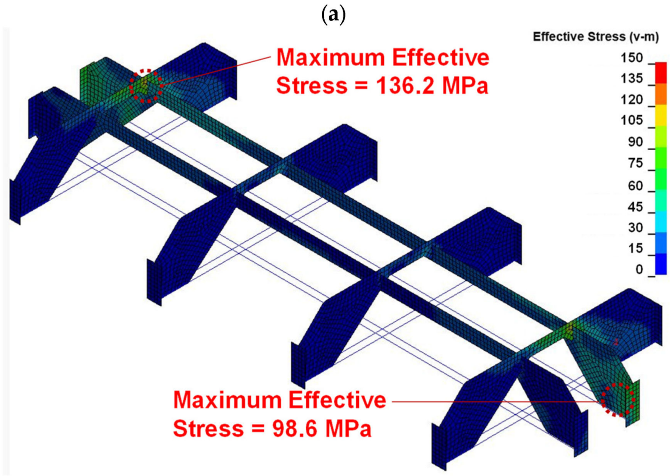

(**b**)

Figure 9. Effective stress distribution of foundation member with optimum retrofit details. (**a**) Finite element model. (**b**) Effective stress of strut–tie retrofit system under service load.

Table 7. Optimum details of strut–tie retrofit system.

Direction	Strut Frame				Tie		
	Steel Type	Yielding Stress (MPa)	Plate Thickness (mm)	Req. Number	Yielding Stress (MPa)	Steel Wire Diameter (mm)	Req. Number (Actual)
Transverse	SS400	235	18	4	400	50	7(8)
Longitudinal			8	2	400	50	6(6)

The optimum retrofit details determined using the FE-based design method are summarized in Table 8. These were compared with those of the strut–tie retrofit details computed using the conventional STM design method. The investigation revealed that the FE-based design method enabled reductions of approximately 55% and 87% in the transverse and longitudinal directions, respectively, compared with the retrofit details determined using the conventional STM design method. It should be noted that the quantities of the retrofit system were computed by multiplying the values for a unit volume of the retrofit system with the required numbers.

Table 8. Comparison between the initial and optimum design.

Direction	Initial Strut–Tie Retrofit System with STM-Based Design Method				Optimum Strut–Tie Retrofit System with FE-Based Design Method				Volume Reduction Ratio (%)
	Unit Area of Strut Frame (mm^2)	t_{pl} (mm)	Req. Number	Total Volume (mm^3)	Unit Area of Strut Frame (mm^2)	t_{pl} (mm)	Req. Number	Total Volume (mm^3)	
Transverse	6.62×10^6	40	4	1.06×10^9	6.62×10^6	18	4	4.77×10^8	55.0%
Longitudinal	9.96×10^6	40	3	1.15×10^6	9.96×10^6	8	2	1.53×10^8	86.7%

4.3. Shear Assessment

The pile-type FE foundation model with the optimum retrofit details evaluated the serviceability of the concrete elements in shear by comparing the maximum shear stress value with the code-defined limit. Figure 10 shows the stress distribution in the Z direction of the concrete solid elements in the transverse and longitudinal directions. This stress distribution reveals that unlike the conventional STM design method (i.e., resisting the shear forces with the strut–tie retrofit system), the retrofit system resists the shear with the concrete elements. To demonstrate the serviceability of the concrete elements under the shear forces, Figure 11 compares the shear stress values determined at the cross-sectional area where the maximum stress is observed with the maximum permissible stress of RC members with shear reinforcements ($\tau_{cc} = 0.37\sqrt{f_{ck}} = 2.19$ MPa) specified in a bridge design code [26,27]. The stress values calculated from the FE simulation were indicated as absolute values. Figure 10 shows that the stress concentration is observed at the loading points and pile locations. However, it is unreasonable to compare the shear stress values generated at certain specific elements with the permissible stress limit (2.19 MPa). Therefore, in this study, the current code-defined permissible stress was compared with the average stress values (indicated using red lines in the figure) of the solid concrete elements in the cross-sectional areas to ensure the serviceability of the concrete elements against shear forces. As shown in Figure 11, the average stress values calculated in the transverse (1.22 MPa) and longitudinal (1.52 MPa) directions did not exceed the permissible stress limits. The standard deviation (SD) values of the simulated data in transverse and longitudinal directions are 2.22 MPa, and 1.51 MPa, respectively. The 84th percentile values (mean + SD) in transverse and longitudinal directions were 3.44 MPa and 3.03 MPa, respectively. The 95th percentile values (Mean + 1.96 SD) is transverse and longitudinal directions were 5.57 MPa and 4.48 MPa, respectively. The 84th and 95th percentile values of the shear stress exceeded the allowable stress limit. This was attributed to the stress concentrations at certain specific elements, which were less than 30% of all solid elements in each direction.

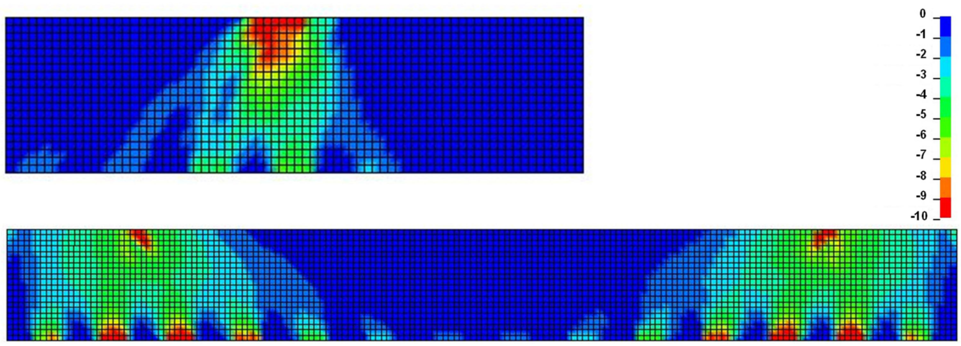

Figure 10. Z direction stress distributions in transverse and longitudinal directions.

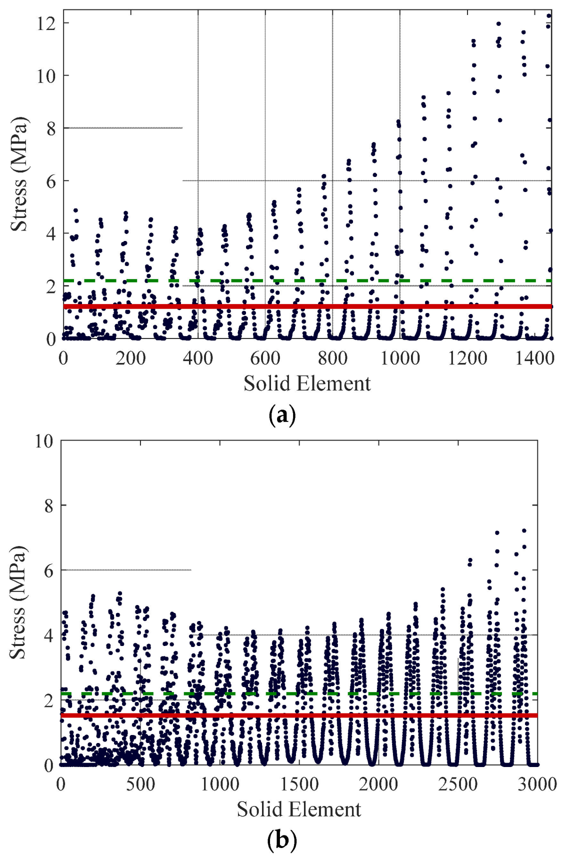

Figure 11. Comparison between Z direction stress and allowable shear stress. (**a**) Transverse direction. (**b**) Longitudinal direction.

5. Conclusions

This study proposed the optimum details of a strut–tie retrofit system for a deep-reinforced concrete foundation member with a reduced thickness. A retrofitting system was developed to minimize the consumption of concrete material (e.g., thickness of the foundation) in deep foundation members. Finite element (FE) models representing mat-type and pile-type foundation members strengthened with a strut–tie retrofit system were developed and simulated under various design loading combinations to estimate the corresponding load-bearing capacities. The initial design details of the strut–tie retrofit system in the foundation member were determined using a code-defined design method with a strut–tie model (STM), and were evaluated in terms of flexure behavior. Subsequently, the effective stress of the strut frame, computed using FE simulations, was compared with the code-defined allowable stress limits to optimize the steel type and strut plate thickness. Finally, the material quantities determined from FE simulations (FE-based design method) were compared with the conventional foundation details obtained using the STM-based design method. The following conclusions were drawn:

(1) The foundation with a strut–tie retrofit system developed using the STM-based design method specified in the current code reduced the thickness of the typical RC foundation by 20%. The numbers of strut–tie retrofit systems in the transverse and longitudinal directions when the strut frame thickness was 40 mm were four and three, respectively. In the FE simulations, the effective stress values obtained from the strut–tie retrofit system did not exceed the permissible stress limit for the LC-1 load combination where the stress values were maximized in all directions (approximately 70% of the permissible stress of LC-1 for SS400 structural steel).

(2) Based on the flexural assessment, a decrease in the plate thickness of the strut–tie retrofit system increased the effective stress in the retrofit system. A decrease in the

number of strut frames led to an increase in the flexural stress. This was attributed to the stress concentration caused by the decrease in the retrofit details. The flexural assessment of the foundation models with reduced material consumption in the strut–tie retrofit system continued until the strut frames exceeded the permissible stress limits specified in the current code.

(3) To optimize the design details of the strut–tie retrofit system (strut plate thickness and structural steel type), the FE simulation results (the maximum effective stress values) for the loading combinations were compared with the permissible stress specified in the current code. The FE simulation results with the loading combinations reveal that SS400 structural steel can be used. Furthermore, the strut plate thickness for the transverse direction (wherein the stress rate is higher than that in the longitudinal direction) is 18 mm. Although the number of strut–tie retrofit systems was reduced from three to two in the longitudinal direction, which had a lower load distribution rate than the transverse direction, the maximum effective stress of the retrofit system did not exceed the permissible stress of the structural steel type until the plate thickness was reduced to 8 mm.

(4) The FE-based design approach can reduce the material consumption of the retrofit details (number of strut frames in the longitudinal direction and the plate thickness) by 55.0% and 86.7% in the transverse and longitudinal directions as compared to the initial details determined from the STM model. The shear and flexural forces of the foundation members with optimum retrofit details under the given loading combinations were estimated to be within the code-defined permissible limits.

(5) Based on the load-bearing capacity assessment, the FE-based design method was more effective in minimizing the material quantities for the strut–tie retrofit system than the conventional design method. The conventional STM-based design method assumes that the arch-shaped strut frames resist the shear produced by the load combinations. However, the FE-based design method implemented for optimizing the retrofit details predicted the actual structural behavior relatively more accurately because it assumed that the concrete and arch-shaped strut frames resisted shear. In a previous study [6], the durability of reinforced concrete members associated with laboratory-based parameters, service life, and raw material demand was reduced due to decreases in the concrete material consumption (20% reduction in the foundation member's thickness). To propose eco-efficient retrofit details, in a future study, a durability-based life-cycle assessment will be conducted for a foundation member installed using a steel strut–tie retrofit system.

Author Contributions: Conceptualization, J.S. and K.L.; methodology, J.S. and K.L.; validation, J.S.; formal analysis, J.S.; investigation, J.S.; resources, K.L.; data curation, J.S.; writing—original draft preparation, J.S.; writing—review and editing, K.L.; visualization, J.S.; supervision, K.L.; project administration, J.S. and K.L.; funding acquisition, K.L. All authors have read and agreed to the published version of the manuscript.

Funding: This research was funded by [the National Research Foundation of Korea (NRF)] grant number [No. NRF-2021R1F1A1059976] and [Cooperative Research Method and Safety Management Technology in National Disaster] grant number [2022-MOIS63-003(RS-2022-ND641021)].

Institutional Review Board Statement: Not applicable.

Informed Consent Statement: Not applicable.

Data Availability Statement: The data that has been used is confidential.

Acknowledgments: This work was supported by the National Research Foundation of Korea (NRF) with a grant funded by the Korean government (MSIT) (No. NRF-2021R1F1A1059976) and Cooperative Research Method and Safety Management Technology in National Disaster funded by Ministry of Interior and Safety (2022-MOIS63-003(RS-2022-ND641021)).

Conflicts of Interest: The authors declare that they have no known competing financial interests or personal relationships that could have appeared to influence the work reported in this paper.

References

1. Yoon, S.M.; Park, H.M.; Park, J.W.; Lee, J.Y. Evaluation of the Structural Behavior of RC Foundations reinforced with Steel Struts. *J. Archit. Inst. Korea-Struct. Constr.* **2009**, *25*, 13–22. (In Korean)
2. Kim, B.H.; Yun, Y.M. An indeterminate strut-tie model and load distribution ratio for RC deep beams-(I) Model & Load Distribution Ratio. *Adv. Struct. Eng.* **2011**, *14*, 1031–1041.
3. Di, H.; Guo, H.; Zhou, S.; Chen, J.; Wen, L. Investigation of the axial force compensation and deformation control effect of servo steel struts in a deep foundation pit excavation in soft clay. *Adv. Civ. Eng.* **2019**, *2019*, 5476354. [CrossRef]
4. Feng, H.H.; Wang, X. Causes and control measures of mass concrete crack of high-rise building basement foundation slab. *Adv. Mater. Res.* **2011**, *163*, 1609–1613. [CrossRef]
5. Müller, H.S.; Haist, M.; Vogel, M. Assessment of the sustainability potential of concrete and concrete structures considering their environmental impact, performance and lifetime. *Constr. Build. Mater.* **2014**, *67*, 321–337. [CrossRef]
6. Li, C.; Li, J.; Ren, Q.; Zheng, Q.; Jiang, Z. Durability of concrete coupled with life cycle assessment: Review and perspective. *Cem. Concr. Compos.* **2023**, *21*, 105041. [CrossRef]
7. Panjehpour, M.; Chai, H.K.; Voo, Y.L. Refinement of strut-and-tie model for reinforced concrete deep beams. *PLoS ONE* **2015**, *10*, e0130734. [CrossRef] [PubMed]
8. Abdul-Razzaq, K.S.; Jebur, S.F. Experimental verification of strut and tie method for reinforced concrete deep beams under various types of loadings. *J. Eng. Sustain. Dev.* **2017**, *21*, 39–55.
9. Farhangi, V.; Karakouzian, M.; Geertsema, M. Effect of micropiles on clean sand liquefaction risk based on CPT and SPT. *Appl. Sci.* **2020**, *10*, 3111. [CrossRef]
10. Stone, R.C.; Farhangi, V.; Fatahi, B.; Karakouzian, M. A novel short pile foundation system bonded to highly cemented layers for settlement control. *Can. Geotech. J.* **2023**. [CrossRef]
11. Kannaujiya, P.; Jaiswal, S.; Chauhan, V.B. Studies on the piled raft foundation for a high-rise building using finite element modeling. In *Advances in Geo-Science and Geo-Structures: Select Proceedings of GSGS 2020*; Springer: Singapore, 2022; pp. 245–252.
12. Schlaich, J.; Schafer, K. Design and detailing of structural concrete using strut-and-tie models. *Struct. Eng.* **1991**, *69*, 113–125.
13. Ramirez, J.A. Strut-Tie Shear Design of Pretensioned Concrete. *Struct. J.* **1994**, *91*, 572–578.
14. ACI Committee 318. *Building Code Requirements for Structural Concrete and Commentary*; ACI 318-05; American Concrete Institute: Farmington Hills, MI, USA, 2005.
15. Liang, Q.Q.; Uy, B.; Steven, G.P. Performance-based optimization for strut-tie modeling of structural concrete. *J. Struct. Eng.* **2002**, *128*, 815–823. [CrossRef]
16. Yun, Y.M.; Ramirez, J.A. Strength of concrete struts in three-dimensional strut-tie models. *J. Struct. Eng.* **2016**, *142*, 04016117. [CrossRef]
17. Xia, Y.; Langelaar, M.; Hendriks, M.A. Optimization-based three-dimensional strut-and-tie model generation for reinforced concrete. *Comput.-Aided Civ. Infrastruct. Eng.* **2021**, *36*, 526–543. [CrossRef]
18. KCI. *KDS 14 20 00*; Korean Concrete Standard Specification. KCI: Seoul, Republic of Korea, 2021.
19. Livermore Software Technology Corporation. *LS-DYNA Keyword User's Manual*, Version 971/R7.0; Livermore Software Technology Corporation: Livermore, CA, USA, 2013.
20. Crawford, J.; Wu, Y.; Choi, H.; Magallanes, J.; Lan, S. *Use and Validation of the Release III K&C Concrete Material Model in LSDYNA*; TR-11-36.6 Technical Report; Karagozian & Case: Glendale, CA, USA, 2012.
21. Wu, Y.; Crawford, J.E. Numerical modeling of concrete using a partially associative plasticity model. *J. Eng. Mech.* **2015**, *141*, 04015051. [CrossRef]
22. Weatherby, J.H. Investigation of Bond Slip between Concrete and Steel Reinforcement under Dynamic Loading Conditions. Ph.D. Thesis, Louisiana State University, Baton Rouge, LA, USA, 2003.
23. Tabiei, A.; Wu, J. Roadmap for crashworthiness finite element simulation of roadside safety structures. *Finite Elem. Anal. Des.* **2000**, *34*, 145–157. [CrossRef]
24. Shin, J.; Stewart, L.K.; Yang, C.S.; Scott, D.W. Implementation of Bond-Slip Performance Models in the Analyses of Non-Ductile Reinforced Concrete Frames Under Dynamic Loads. *J. Earthq. Eng.* **2020**, *24*, 129–154. [CrossRef]
25. MOLIT. *Railway Design Standard of the Ministry of Land, Infrastructure, and Transport*; MOLIT: Seoul, Republic of Korea, 2015.
26. Ghosn, M.; Moses, F. *NCHRP Report 489: Design of Highway Bridge for Extreme Events*; Transportation Research Board of the National Academies; Transportation Research Board: Washington, DC, USA, 2003.
27. Korea Bridge Design Code. *Limit-State-Based Bridge Design Specifications*; Korea Road and Transportation Association: Seoul, Republic of Korea, 2012.